



Unlocking Benzosampangine's Potential: A Computational Approach to Investigating, Its Role as a PD-L1 Inhibitor in Tumor Immune Evasion via Molecular Docking, Dynamic Simulation, and ADMET Profiling

Bioinformatics and Biology Insights
Volume 18: 1–18
© The Author(s) 2024
Article reuse guidelines:
sagepub.com/journals-permissions
DOI: 10.1177/11779322241298591


Abderrahim Ait Ouchouai^{1,2,*}, Salah Eddine El Hadad^{1,2,*},
Marouane Aherkou^{2,3}, Elkamili Fadoua⁴, Mkamel Mouad²,
Youssef Ramli⁵, Anass Kettani⁶ and Ilhame Bourais^{1,2,7} 

¹Mohammed VI University of Sciences and Health (UM6SS), Casablanca, Morocco. ²Mohammed VI Center for Research and Innovation (CM6RI), Rabat, Morocco. ³Biotechnology Laboratory (MedBiotech), Bioinova Research Center, Rabat Medical and Pharmacy School, Mohammed V University in Rabat, Rabat, Morocco. ⁴Rabat Medical and Pharmacy School, Mohammed Vth University, Rabat, Morocco. ⁵Laboratory of Medicinal Chemistry, Drug Sciences Research Center, Faculty of Medicine and Pharmacy, Mohammed V University in Rabat, Rabat, Morocco. ⁶Laboratory of Biology and Health, URAC 34, Faculty of Sciences Ben M'sik, Health and Biotechnology Research Center, Hassan II University of Casablanca, Casablanca, Morocco. ⁷Laboratory of Human Pathologies Biology, Department of Biology, Faculty of Sciences, Mohammed V University in Rabat, Rabat, Morocco.

*Abderrahim Ait Ouchouai and Salah Eddine El Hadad contributed equally to this work.

ABSTRACT: The interaction between programmed cell death protein 1 (PD-1) and its ligand PD-L1 plays a crucial role in tumor immune evasion, presenting a critical target for cancer immunotherapy. Despite being effective, current monoclonal antibodies present some drawbacks such as high costs, toxicity, and resistance development. Therefore, the development of small-molecule inhibitors is necessary, especially those derived from natural sources. In this study, benzosampangine is predicted as a promising PD-L1 inhibitor, with potential applications in cancer immunotherapy. Utilizing the high-resolution crystal structure of human PD-L1 (PDB ID: 5O45), we screened 511 natural compounds, identifying benzosampangine as a top candidate with exceptional inhibitory properties. Molecular docking predicted that benzosampangine exhibits a strong binding affinity for PD-L1 (−9.4 kcal/mol) compared with established controls such as CA-170 (−6.5 kcal/mol), BMS-202 (−8.6 kcal/mol), and pyrvinium (−8.9 kcal/mol). The compound's predicted binding efficacy is highlighted by robust interactions with key amino acids (ILE54, TYR56, GLN66, MET115, ILE116, SER117, ALA121, ASP122) within the active site, notably forming 3 Pi-sulfur interactions with MET115—an interaction absent in control inhibitors. In addition, ADMET profiling suggests that over the control molecules, benzosampangine has several key advantages, including favorable solubility, permeability, metabolic stability, and low toxicity, while adhering to Lipinski's rule of five. Molecular dynamic simulations predict the stability of the benzosampangine-PD-L1 complex, reinforcing its potential to sustain inhibition of the PD-1/PD-L1 pathway. MMGBSA analysis calculated a binding free energy (ΔG_{bind}) of −39.39 kcal/mol for the benzosampangine-PD-L1 complex, with significant contributions from Coulombic, lipophilic, and Van der Waals interactions, validating the predicted docking results. This study investigates *in silico* benzosampangine, predicting its better molecular interactions and pharmacokinetic profile compared with several already known PD-L1 inhibitors.

KEYWORDS: PD-1/PD-L1 inhibitors, benzosampangine, molecular docking, molecular dynamic, small molecules, *in silico* study, cancer

RECEIVED: April 8, 2024. **ACCEPTED:** October 21, 2024.

TYPE: Research Article

FUNDING: The author(s) received no financial support for the research, authorship, and/or publication of this article.

DECLARATION OF CONFLICTING INTERESTS: The author(s) declared no potential conflicts of interest with respect to the research, authorship, and/or publication of this article.

CORRESPONDING AUTHOR: Ilhame Bourais, Mohammed VI Center for Research and Innovation (CM6RI), Boulevard Mohamed Al Jazouli, Madinat Al Irfane, Hay Riad, Rabat 10000, Morocco. Email: ibourais@cm6.ma

Introduction

T lymphocyte immunity plays a vital role in maintaining the body's homeostasis through the selective recognition and elimination of abnormal cells, including cancer cells.^{1,2}

Tumor cells initiate the cancer-immunity cycle by releasing tumor antigens.³ Antigen-specific T cells first recognize tumor antigens presented by major histocompatibility complexes (MHCs) on antigen-presenting cells (APCs), leading to their priming and activation. Once activated and proliferated, T cells migrate to specific sites guided by chemokine concentration

gradients.⁴ Following costimulatory signals between T cells and APCs to achieve optimal activation, immune checkpoints like PD1 and its ligand PDL1 are involved to play a crucial role in preventing excessive T-cell activation.^{3,5} On recognizing the same antigen on MHCs, T cells release IFN- γ to enhance the efficiency of tumor cell destruction. IFN- γ released from CD8⁺ T cells upregulates the expression of PDL1 on tumor cells^{6,7} (Figure 1). Meanwhile, T-cell receptor signaling upregulates the expression of PD1 on the T cell surface which binds to PDL1 to exert negative regulatory effects and blunt the



Creative Commons Non Commercial CC BY-NC: This article is distributed under the terms of the Creative Commons Attribution-NonCommercial 4.0 License (<https://creativecommons.org/licenses/by-nc/4.0/>) which permits non-commercial use, reproduction and distribution of the work without

further permission provided the original work is attributed as specified on the SAGE and Open Access pages (<https://us.sagepub.com/en-us/nam/open-access-at-sage>).

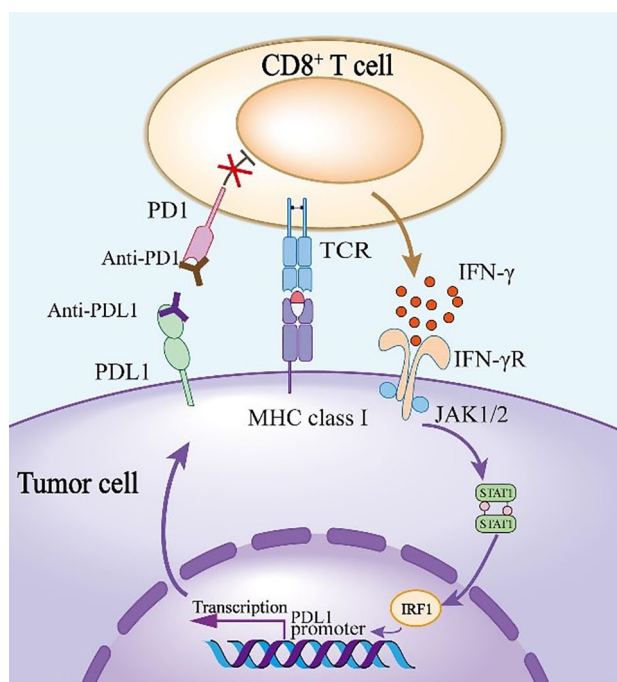


Figure 1. Mechanism of PD1/PD-L1 blockade. The CD8⁺ T cell activates on recognizing the tumor antigen presented on MHC class I and releases IFN- γ to bind to IFN- γ receptor, and consequently induces the expression of PDL1 on tumor cells. PDL1 conjugates the elevated PD1 on T cell surface, triggering inhibitory effect of PD1/PD-L1 axis. Anti-PD1 or anti-PDL1 antibody blocks the interaction of PD1 and PD-L1, and abolishes the inhibition of CD8⁺ T cell thus enhancing the antitumor activity.⁴

antitumor function of T cells.⁸⁻¹⁰ Multiple studies have shown that PD-L1 is overexpressed in various types of cancers, including breast, lung, gastric, papillary thyroid, bladder, testicular, colorectal, melanoma, non-small cell lung (NSCLC), head and neck, and kidney cancers.¹¹⁻¹³ The interaction between PD-L1 and PD-1 contributes to the maintenance of an immunosuppressive tumor environment by suppressing T lymphocyte function leading to proliferation and cytokine secretion reduction which impairs their ability to destroy tumor cells.¹⁴⁻¹⁶ In addition, this interaction induces apoptosis of T lymphocytes promoting tumor cell survival.^{17,18} Tumor environment cells also express PD-L1, using this pathway to evade the immune system.^{16,19,20} As a result, blocking immune checkpoint pathways has become an important strategy for reversing the immunosuppressive mechanisms employed by tumor cells to reactivate the immune system, and targeting the PD-1/PD-L1 pathway is considered a frequently used approach.^{21,22} Clinical trials involving anti-PD-L1 agents have yielded encouraging results among cancer patients, including renal cell carcinoma, melanoma, NSCLC and metastatic urothelial bladder cancer.^{11,23,24} Currently, multiple monoclonal antibodies have been approved by the Food and Drug Administration (FDA) as inhibitory drugs impeding the PD-1-PD-L1 interaction in cancer therapy.^{23,25-28} Two anti-PD-1 antibodies, pembrolizumab (humanized IgG4 antibody) and nivolumab (human

IgG4 antibody), are approved as the second line for the treatment of Hodgkin lymphoma, NSCLC, metastatic melanoma, head and neck squamous cell carcinoma, and kidney cancer.^{26,29-32} As for anti-PD-L1 antibodies, atezolizumab (humanized IgG1 antibody) is approved for the treatment of advanced NSCLC and urothelial carcinoma,^{25,33} whereas durvalumab (human IgG1 antibody) and avelumab (human IgG1 antibody) have been approved by the FDA and have shown positive responses in the treatment of various malignant tumors, including metastatic NSCLC, melanoma, urothelial carcinoma, and Merkel cell carcinoma.³⁴⁻³⁶ However, monoclonal antibodies have drawbacks, including low stability, high manufacturing costs, low tumor penetration rates, difficulty in overcoming biological barriers, lack of oral availability, and potential immunogenic side effects.³⁷⁻³⁹ Therefore, it is necessary to overcome these disadvantages through the development of new small, stable, and more effective inhibitory molecules with the ability to bind to PD-L1 and block the PD-1/PD-L1 interaction without inducing undesirable effects. In this study, we suggest that targeting PD-L1 with small natural molecules could effectively block the PD1-PD-L1 interaction and consequently reactivate the immune system. The use of natural compounds derived from medicinal plants holds great promise for the development of therapeutic medicines that are both less harmful and more effective. Numerous studies have previously shown the therapeutic power of natural molecules.⁴⁰⁻⁴³ In this regard, we first performed a virtual screening of a database of natural compounds and their derivatives against the crystalline structure of PD-L1 available in the Protein Data Bank (PDB; PDB code: 5O45) to discover potential inhibitors of PD-L1, followed by molecular dynamics (MD) simulations to assess the stability of the complexes. This approach has been adopted in several previous studies.⁴⁴⁻⁴⁹

Materials and Methods

Data collection and ligand preparation

A local database of 511 natural compounds and their derivatives (inhibitors) was assembled from various essential oils derived from medicinal plants and subjected to screening to identify potential compounds that inhibit the interaction between PD-1 and PD-L1 in cancer. The ligands obtained from the PubChem database⁵⁰ in 3D SDF format were prepared using AutoDockTools;⁵¹ Gasteiger charges were assigned and stored in PDBQT format.

Receptor preparation and receptor grid generation

The 3-dimensional crystal structure of human PD-L1 in complex with an inhibitor (PDB ID: 5O45) was utilized for docking studies. This particular structure was chosen for its high resolution (0.99Å) providing a precise and a detailed representation of the protein's atomic structure. The inhibitor-bound form of PD-L1 ensures that the binding conformation

is well-defined, enabling a more reliable identification of potential inhibitors among the screened compounds. Subsequently, heteroatoms were deleted, water molecules were eliminated, and Kollman atomic charges, along with polar hydrogens, were incorporated into the receptors using AutoDockTools.⁵¹ The prepared structure, ready for molecular docking studies, was saved in AutoDock PDBQT format.

Molecular docking protocols

To identify inhibitors of the interaction between PD-1 and PD-L1, molecular docking studies were performed to screen 511 natural molecules and their derivatives against the active site of the PD-L1 protein using the AutoDock Vina docking program. For the PD-L1 target, a grid box (X: 40Å, Y: 40Å, and Z: 40Å) was created to encompass the binding pocket highlighted by CB-Dock2 (<https://cadd.labshare.cn/cb-dock2/php/blinddock.php>).⁵² The center of the grid box was set at (X: 10.441, Y: 6.855, Z: -18.463), and the other AutoDock Vina parameters were maintained at their default values (energy range = 4 and exhaustiveness = 8). The ligands' binding affinities to the target's active site were expressed in kcal/mol units.

Drug-likeness prediction

The ligands with the highest affinities were selected for drug-likeness assessment. This evaluation was carried out using the free online tool Swiss ADME (<http://www.swissadme.ch/>), developed by the Swiss Institute of Bioinformatics.⁵³ We based our assessment on Lipinski's rule of five (Ro5) to predict the bioavailability of molecules.^{54,55} The Ro5 introduced the criteria of the number of rotatable bonds, the molecular weight, the number of hydrogen bond acceptors, the number of hydrogen bond donors, and the octanol-water partition coefficient. A molecule is considered drug-like if it meets at least 4 of the 5 cited criteria.⁵⁴

Toxicity analysis

Computational methods facilitated the evaluation of a safety profile for the compounds studied. Ligands exhibiting drug-like properties were selected for toxicity prediction. The ProTox-II (https://tox-new.charite.de/protox_II/) server was used to assess the toxic effects of the chosen compounds.⁵⁶ This server predicts organ toxicity (hepatotoxicity), as well as various toxicological endpoints (carcinogenicity, immunotoxicity, cytotoxicity, and mutagenicity) and the median lethal dose (LD50) for the selected molecules.

Post-docking analysis and visualization

Molecules not showing toxicity in ProTox-II were selected for receptor-ligand interaction analysis to validate their interaction with active site residues of the target. Discovery Studio was used to perform post-docking visualization 2D.⁵⁷

Molecular dynamics simulations

By incorporating the classical Newton equation of motion, MD simulations generally simulate the movements of atoms over time and predict the binding state of ligands in the physiological environment.⁵⁸ A study of MD simulations was conducted with the docking complex of PD-L1_benzosampangine over 100 ns using Schrödinger LLC Desmond software.⁵⁹ The TIP3P solvent model (Intermolecular Interaction Potential 3 Points Transferable), based on an orthorhombic box, was used at a temperature of 300 K, a pressure of 1 atm, and an OPLS_2005 force field.⁶⁰ Using counter-ions and 0.15 M sodium chloride, the models were, respectively, neutralized and simulated under physiological conditions. The models were equilibrated before the simulation, and the trajectories were stored for inspection every 100 ps.

MMGBSA calculations

During MD simulations, the binding free energy (ΔG_{bind}) of the docked complex was determined using the MMGBSA module (Suite Schrodinger, LLC, New York, NY, 2017-4). The calculations were performed using simultaneously, the OPLS 2005 force field, the VSGB solvent model and rotamer search techniques.⁶¹ MD trajectory frames were chosen at each 10 ns interval after MD execution. The following equation was used to calculate the total binding free energy:

$$\Delta G_{\text{bind}} = G_{\text{complex}} - (G_{\text{protein}} + G_{\text{ligand}})$$

where ΔG_{bind} = binding free energy, G_{complex} = free energy of the complex, G_{protein} = free energy of the target protein, and G_{ligand} = free energy of the ligand.

Pharmacokinetics (ADME) and toxicity prediction

The ADMET results used in this study were obtained from the ADMETlab 2.0 server,⁶² a widely recognized platform for predicting pharmacokinetic and toxicity properties of chemical compounds. We focused on evaluating the key ADMET properties crucial for assessing the potential of drug candidates, including physicochemical properties, medicinal chemistry parameters, absorption, distribution, metabolism, excretion, and toxicity. ADMETlab 2.0 employs a multitask graph attention framework for robust and accurate prediction models. The server's batch computation module and optimized result representation enhance usability. Using ADMETlab 2.0, we sought to gain insights into the pharmacokinetic and toxicity profiles of compounds to optimize drug candidate screening. The freely accessible ADMETlab 2.0 server is a valuable online platform for early-stage drug discovery.⁶²

Results

In this study, we screened 511 natural compounds for their potential inhibitory effects on the PD-L1 receptor using a structure-based drug design approach. The PD-L1 receptor was chosen for its pivotal role in immune checkpoint pathways,

which are essential for the regulation of immune responses. Inhibiting PD-L1 can enhance antitumor immunity by preventing its interaction with PD-1, thus making it a valuable target for cancer immunotherapy. In our docking study, we used the 3-dimensional crystal structure of human PD-L1 in a complex with an inhibitor (PDB ID: 5O45). This particular structure was selected because of its high resolution (0.99Å), which provides an accurate and detailed representation of the protein's atomic structure. The inhibitor-bound form of PD-L1 ensures well-defined binding conformation, enabling more reliable identification of potential inhibitors from the screened compounds. During the screening, compounds were evaluated based on their ability to interact with the active site residues of PD-L1. This criterion is a key factor in achieving effective disruption of the PD-1/PD-L1 interaction. In addition, compounds were assessed for their drug-like properties, nontoxicity, and stability of the complexes formed with PD-L1 in MD simulations. These criteria are essential to ensure that the selected compounds not only have the potential to effectively inhibit PD-L1, but also have the favorable pharmacokinetic and pharmacodynamic profiles required for further development as therapeutic agents. Compounds that interact favorably with PD-L1 active site residues, have drug-like properties, are non-toxic, and form stable complexes in MD simulations were considered as potential active inhibitors of PD-L1. These candidates were selected for further experimental validation, highlighting their potential as promising therapeutic agents in cancer immunotherapy.

The following residues of PD-L1, ILE54, TYR56, MET115, ILE116, SER117, ALA121, ASP122, and TYR123, have been reported in various studies to contribute to the interaction between PD-L1 and PD-1.⁶³⁻⁶⁷ The Cb-Dock2 tool was used to identify the binding pocket of PD-L1. The binding site is illustrated in Figure 2.

Molecular docking is a critical step in structure-based drug design. In this study, molecular docking simulations were carried out employing the AutoDock Vina program to evaluate the potential of small natural molecules to inhibit the interaction between PD-1 and PD-L1 for immune system reactivation. We set -9 kcal/mol as the threshold binding energy value to select only molecules that strongly engage the PD-L1 active site.⁶⁸ Table 1 presents the binding energy values for the top 23 ligands among the 511 screened compounds, where their binding energies (below -9 kcal/mol) indicate a strong affinity for the PD-L1 target. Kaempferol 3-(6'-galloyl)galactoside and Z-guggulsterone exhibited the best binding energy toward the target (-9.8 kcal/mol), implying their strong interaction with the binding pocket residues. The binding energy values and binding poses for the top-docked compounds are summarized in Table 1.

Lipinski's rule of five is applied to determine whether a molecule has the appropriate properties to qualify as a potential active pharmaceutical ingredient for oral administration. We

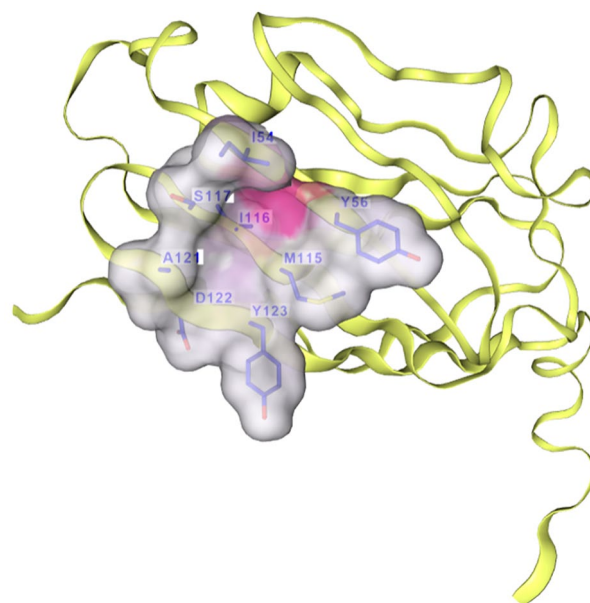








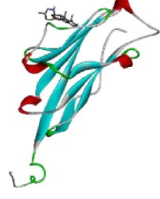
Figure 2. The predicted binding pocket of PD-L1. Key residues represented in blue in the binding pocket and the surfaces of the binding pocket in PD-L1 are presented in gray.

assessed the drug-likeness properties of the molecules with the best docking scores (Table 1) to exclude compounds that are unsuitable for further developmental research. As shown in the table below (Table 2), 17 out of the 23 studied compounds adhered to Ro5, suggesting that these molecules are promising drug candidates. Only Kaempferol 3-(6'-galloyl)galactoside, amentoflavone, hypericin, pseudohypericin, beta-carotene, and hesperidin showed 2 or more violations. The detailed properties of each molecule are reported in Table 2.

Toxicity was assessed by considering various targets associated with adverse effects of drugs to exclude any toxic compounds from the study. The compounds studied had to be inactive on all targets with a high LD50. Benzosampangine showed no signs of toxicity, with LD50 value equal to 2000 mg/kg. However, Z-guggulsterone, enoxolone, chelerythrine, and finasteride are both carcinogenic and immunogenic. While, veratramine, tomatidine, benzo[c]phenanthridine, limonin, peiminine, and finasteride exhibited low LD50 values of 315, 500, 331, 244, 280, and 418 mg/kg, respectively, indicating their potential toxicity. The detailed toxicological properties of each molecule are reported in Table 3.



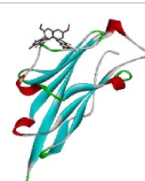
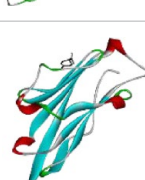
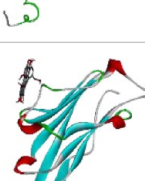
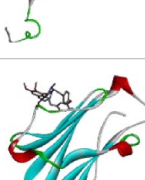

Various interactions were observed between benzosampangine and the PD-L1 protein structure. As shown in Figure 3, benzosampangine engaged with several residues in PD-L1 active site, indicating a strong binding affinity. Specifically, it demonstrated Van der Waals interactions with ILE54, GLN66, ILE116, ASP122, and TYR123. Although individually weak, these Van der Waals forces collectively provide substantial stabilization to the ligand-receptor complex by creating extended contact surfaces. A carbon-hydrogen bond

Table 1. Molecular docking results and binding poses of top docked compounds with PD-L1 structure.

COMPOUNDS	AFFINITY (KCAL/MOL)	PUBCHEM CID	BINDING POSES
Kaempferol 3-(6''-galloylgalactoside)	-9,8	5280863	
Z-guggulsterone	-9,8	6450278	
Veratramine	-9,7	6070	
Amentoflavone	-9,6	5281600	
Hypericin	-9,4	3663	
Taraxerol	-9,4	92097	
Tomatidine	-9,4	65576	


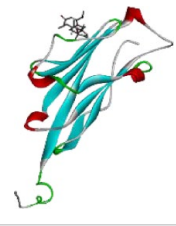



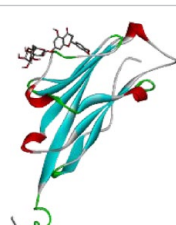

(Continued)

Table 1. (Continued)

COMPOUNDS	AFFINITY (KCAL/MOL)	PUBCHEM CID	BINDING POSES
Benzo(4,5)sanpangine	-9,4	383960	
Benzo[c]phenanthridine	-9,3	344234	
Isoginkgetin	-9,3	5318569	
Limonin	-9,3	179651	
Pseudohypericin	-9,3	4978	
Berbamine	-9,2	275182	
Beta-carotène	-9,2	5280489	

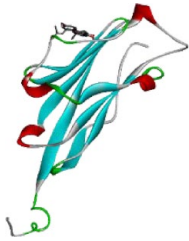

(Continued)

Table 1. (Continued)

COMPOUNDS	AFFINITY (KCAL/MOL)	PUBCHEM CID	BINDING POSES
Enoxolone	-9,2	10114	
Officinatrione	-9,2	71567452	
Sophoradin	-9,2	5321393	
Taraxasterol	-9,2	115250	
Chelerythrine	-9,1	2703	
Hesperidin	-9,1	10621	
Peiminine	-9,1	167691	

(Continued)

Table 1. (Continued)

COMPOUNDS	AFFINITY (KCAL/MOL)	PUBCHEM CID	BINDING POSES
Lupinifolin	-9	10 250 777	
Finasteride	-9	57363	

with SER117 enhances the specificity and stability of the binding interaction. Hydrogen bonds are crucial for maintaining the proper orientation and binding affinity of the ligand in the active site, often contributing significantly to the overall binding energy. Notably, benzosampangine forms 3 Pi-sulfur interactions with MET115. These interactions are significant as they involve the aromatic ring system of benzosampangine interacting with the sulfur atom of methionine. Although less common, Pi-sulfur interactions provide strong noncovalent interactions that can significantly stabilize the ligand in the binding pocket, contributing to the high binding affinity observed. Moreover, benzosampangine and TYR56 form numerous Pi-Pi stacked interactions. The relevance of these interactions in providing significant binding energy is attributed to the overlap of π -orbitals between aromatic rings. This type of interaction is essential for preserving the structural integrity of the ligand-protein complex and enhancing binding specificity. The complex was further stabilized by hydrophobic interactions ensured by Pi-alkyl interactions observed on ALA121. Through the establishment of hydrophobic interaction, non-polar regions of the ligand play a crucial role in enhancing overall binding affinity and stability of the complex. In summary, these interactions suggest that benzosampangine effectively binds to critical residues of the PD-L1 active site and potentially may inhibit the interaction between PD-L1 and PD-1. The interaction profile emphasizes benzosampangine potential as a candidate for further experimental validation and promising therapeutic development in cancer diseases.

We also explored the dynamic behavior of the complex interactions through MD simulations between the target receptor PD-L1 and benzosampangine over 100 ns, a sufficient time for the dynamic behavior of C α atoms within the complex. This duration allows the assessment of the conformational stability of the compound-PD-L1 complex and its

changes under physiological conditions. Various parameters were analyzed to validate the stability of the complex studied, including root mean square deviation (RMSD), root mean square fluctuation (RMSF), protein secondary structure, and protein-ligand contact analysis. The RMSD graph allows the assessment of the compound-PD-L1 complex stability throughout the 100 ns simulation. A complex with a low RMSD value is considered stable, whereas a higher RMSD suggests potential instability. Typically, RMSD values within the range of 1Å to 3Å are acceptable, but significantly larger changes suggest that the protein undergoes substantial conformational changes during the simulation. The RMSD values should stabilize around a fixed value. If the protein's RMSD continues to either increase or decrease on average toward the end of the simulation, it suggests that the system has not reached equilibrium, and the simulation duration may be insufficient for a thorough analysis. In our study, the RMSD graph for the benzosampangine-PD-L1 complex is presented in Figure 4. The average RMSD of the protein alone was 4.08Å, which decreased to 1.52Å after binding with benzosampangine. This decrease indicates that the binding of benzosampangine increased the stability of the PD-L1 protein. Increased protein stability upon ligand binding is often correlated with effective inhibition because a stable complex formation implies that the ligand is well accommodated within the binding site, resulting in minimal conformational changes. This stability can support the ligand's ability to effectively block or inhibit the function of the protein, in our case, PD-L1. A stable PD-L1-benzosampangine complex supports that benzosampangine may maintain its inhibitory interactions over time, reducing the likelihood of PD-L1 interacting with its natural binding partners, such as PD-1. The observed stability, despite initial fluctuations due to system equilibration during the first nanoseconds, remained consistent throughout the simulation. A

Table 2. Predicted drug likeness of PD-L1 potential inhibitors.

COMPOUNDS	LIPINSKI'S RULE OF FIVE					LOGP (<5)	VIOLATIONS
	MOLECULAR WEIGHT (<500 DA)	NO. ROTATABLE BONDS (<15)	NO. H-BOND DONORS (5)	NO. H-BOND ACCEPTORS (<10)			
Kaempferol 3-(6''-galloylgalactoside)	600,5	7	8	15	0,3	3	
Z-guggulsterone	312,45	0	0	2	4,03	0	
Veratramine	409,6	2	3	3	4,3	1	
Amentoflavone	538,46	3	6	10	3,62	2	
Hypericin	504,44	0	6	8	4,26	2	
Taraxerol	426,72	0	1	1	7,22	1	
Tomatidine	415,65	0	2	3	5,9	1	
Benzo(4,5)sanpangine	282,3	0	0	3	3,37	0	
Benzo[c]phenanthridine	229,28	0	0	1	4	0	
Isoginkgetin	566,51	5	4	10	4,39	1	
Limonin	470,51	1	0	8	2,55	0	
Pseudohypericin	540,44	1	7	9	3,5	2	
Berbamine	609,78	3	1	8	5,15	1	
Beta-carotène	536,78	10	0	0	11,11	2	
Enoxolone	470,68	1	2	4	5,17	1	
Officinatrione	454,68	1	0	3	5,91	1	
Sophoradin	460,6	9	3	4	6,8	1	
Taraxasterol	426,72	0	1	1	7,14	1	
Chelerythrine	348,37	2	0	4	3,02	0	
Hesperidin	610,56	7	8	15	-0,72	3	
Peiminine	429,64	0	2	4	3,52	0	
Lupinifolin	406,47	3	2	5	4,38	0	
Finasteride	372,54	3	2	2	3,29	0	

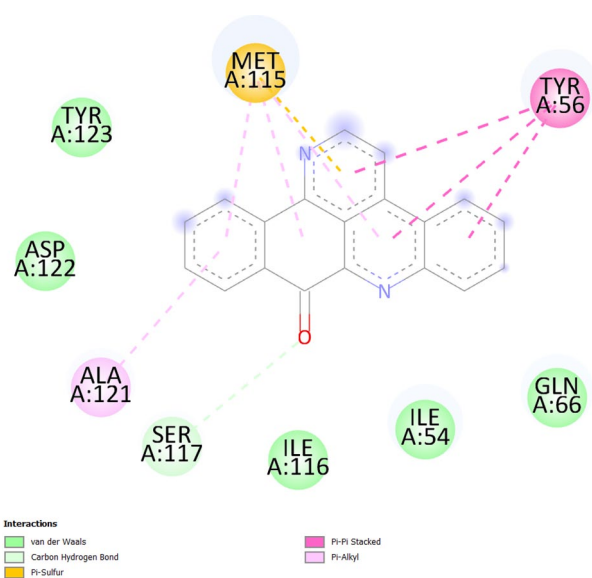
fluctuation at 84 ns did not exceed 3Å, indicating that the system was well-balanced throughout the simulation duration. This consistent stability reinforces the potential of benzosampangine as a promising inhibitor of PD-L1, suggesting its potential for further experimental validation and therapeutic development.

The RMSF measurement characterizes the local changes in protein chains during the simulation revealing the rigidity and flexibility of the protein's amino acids. Peaks indicate the residues of the protein that fluctuate during the simulation. Typically, secondary structure elements (alpha helices and beta strands) are rigid and fluctuate less than (N- and C-terminal) regions, which are flexible. The RMSF graph of the system (Figure 5) demonstrates that the residues interacting with benzosampangine, highlighted by green bars, exhibit fluctuations

decrease compared with other regions. This variation suggests that the binding of benzosampangine stabilizes these residues, resulting in increased rigidity and decreased mobility. Specifically, residues such as MET115, TYR56, ALA121, SER117, TYR123, ASP122, ILE116, ILE54, and GLN66, which interact directly with benzosampangine, are involved in this stabilization process. In contrast, other regions did not interact with benzosampangine, particularly those around residues 25-35 and 45-55, and showed higher fluctuations. These areas are more flexible, likely due to the lack of stabilizing interactions with the ligand. This flexibility is characteristic of regions not implied in direct ligand binding, allowing them to move more freely during the simulation. These observations underline the critical role of the identified residues in ligand binding and protein stability. The interactions between

Table 3. Organ toxicity and toxicological endpoints predicted activities.

COMPOUNDS	TOXICITY					
	HEPATOXICITY	CARCINOGENICITY	IMMUNOTOXICITY	MUTAGENICITY	CYTOTOXICITY	LD ₅₀ (MG/KG)
Z-guggulsterone	Inactive	Active	Active	Inactive	Inactive	2300
Veratramine	Inactive	Inactive	Active	Inactive	Inactive	315
Taraxerol	Inactive	Inactive	Active	Inactive	Inactive	70000
Tomatidine	Inactive	Inactive	Active	Inactive	Inactive	500
Benzosampangine	Inactive	Inactive	Inactive	Inactive	Inactive	2000
Benzo[c]phenanthridine	Inactive	Inactive	Inactive	Active	Inactive	331
Isoginkgetin	Inactive	Inactive	Active	Inactive	Inactive	4000
Limonin	Inactive	Inactive	Active	Inactive	Inactive	244
Berbamine	Inactive	Inactive	Active	Active	Inactive	1700
Enoxolone	Inactive	Active	Active	Inactive	Inactive	560
Officinatrione	Inactive	Inactive	Active	Inactive	Inactive	5000
Sophoradin	Inactive	Inactive	Active	Inactive	Inactive	1000
Taraxasterol	Inactive	Inactive	Active	Inactive	Inactive	5000
Chelerythrine	Inactive	Active	Active	Active	Active	778
Peiminine	Inactive	Inactive	Active	Inactive	Inactive	280
Lupinifolin	Inactive	Inactive	Active	Inactive	Inactive	2000
Finasteride	Inactive	Active	Active	Inactive	Inactive	418

**Figure 3.** 2D interaction of benzosampangine with the active site of PD-L1.

benzosampangine and these key residues contribute to the overall stability of the PD-L1 protein-ligand complex, enhancing the inhibitory potential of benzosampangine.

The variations in the secondary structure elements (% SSE) of PD-L1, including alpha helices and beta strands, were assessed over simulation time. The plot at the top summarizes the SSE composition for each trajectory frame over the course of the simulation and the plot at the bottom tracks each residue and its SSE assignment over time, with variations represented in orange and blue corresponding to alpha helices and beta sheets, respectively (Figure 6). The percentage of beta strands is notably higher compared with the percentage of alpha helices. However, the overall secondary structure elements of the PD-L1 protein remained stable at approximately 44% throughout the simulation. This consistency suggests that no significant structural changes occurred and the integrity of the PD-L1 structure was maintained during its interaction with benzosampangine.

The interaction types between benzosampangine and the protein were monitored throughout the simulation to assess their contribution to the stability of the complex. These interactions include hydrophobic, hydrogen bonds, water bridges, and ionic interactions and are illustrated in Figure 7. The results indicate that hydrophobic interactions, hydrogen bonds, and water bridges were the most frequently observed ligand-protein interactions. Benzosampangine engaged with all residues in the active site of PD-L1. Particularly, the hydrophobic

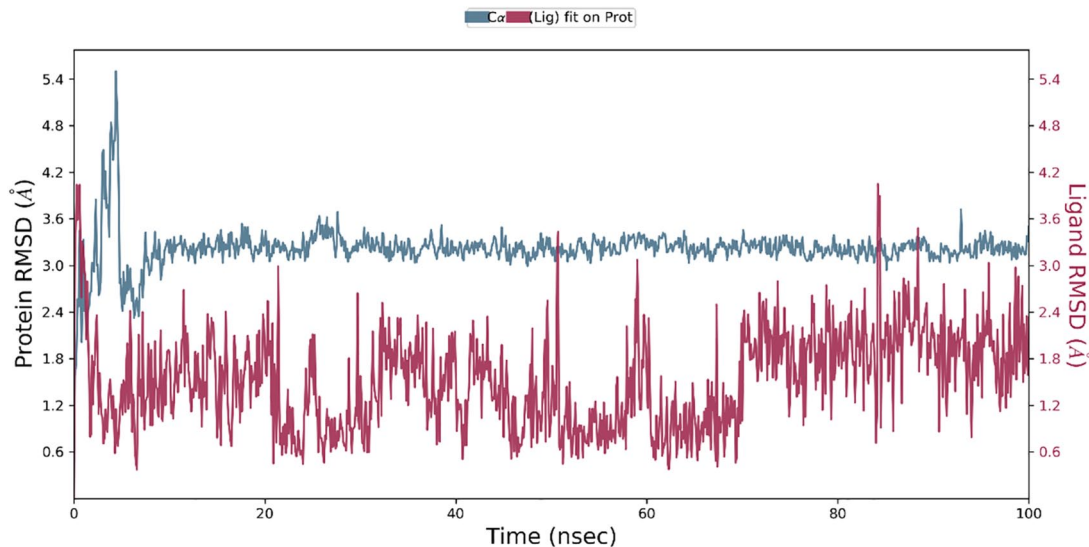


Figure 4. Root mean square deviation (RMSD) of the protein PD-L1 alone (blue) and in complex with and benzosampangine (red) as a function of simulation time.

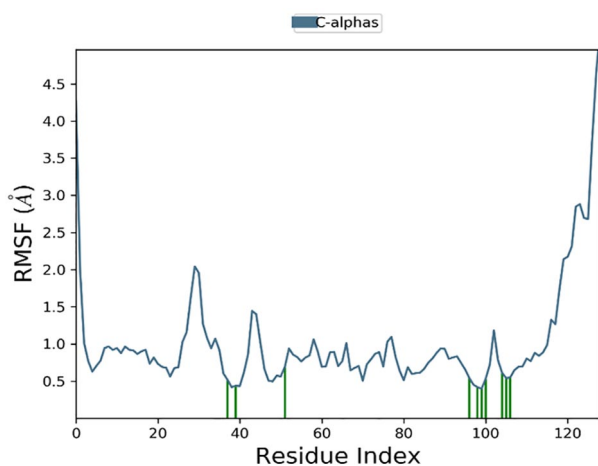


Figure 5. Root mean square fluctuation (RMSF) analysis of PD-L1 in complex with benzosampangine. The vertical green lines represent the amino acid residue of RPFC making contact with ligand.

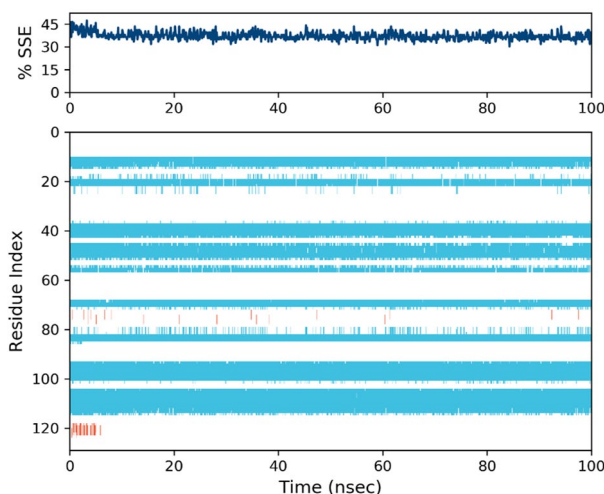


Figure 6. The stability of PD-L1's secondary structure over 100 ns of MD simulation in complex with benzosampangine.

interaction with TYR56, the strongest interaction observed, remained stable for approximately 50% of the simulation time. These findings highlight the stability of the benzosampangine-PD-L1 complex.

All results from the MD indicate the stability of benzosampangine when complexed with the PD-L1 protein. This observed stability suggests that benzosampangine may have the potential to inhibit the interaction between PD-L1 and PD-1 under physiological conditions.

Molecular Mechanics-Generalized Born Surface Area (MM-GBSA) analysis allows us to identify the binding efficiency of the ligand with the receptor, by calculating the binding free energy of the protein-ligand complex at the molecular level. This approach is highly beneficial for the validation of docking and MD simulation results. The binding free energy

(ΔG_{bind}) of benzosampangine to PD-L1 is equal to -39.39 kcal/mol (Table 4). ΔG_{bind} is influenced by nonbonded interactions such as $\Delta G_{\text{bindCoulomb}}$, $\Delta G_{\text{bindCovalent}}$, $\Delta G_{\text{bindHbond}}$, $\Delta G_{\text{bindLipo}}$, $\Delta G_{\text{bindSolvGB}}$, and $\Delta G_{\text{bindvdW}}$. The contribution of each interaction is detailed in Table 4. The $\Delta G_{\text{bindCoulomb}}$, $\Delta G_{\text{bindLipo}}$, and $\Delta G_{\text{bindvdW}}$ energies contributed significantly to reach the average binding energy, compared with the $\Delta G_{\text{bindCovalent}}$ and $\Delta G_{\text{bindSolvGB}}$ energies which showed an unfavorable energetic contribution to the final binding energies average. Thus, the binding energy observed in docking studies is well-supported by the MM-GBSA calculations derived from the MD simulation trajectories.

Benzosampangine presents a compelling profile in terms of its absorption, distribution, metabolism, excretion, and toxicity

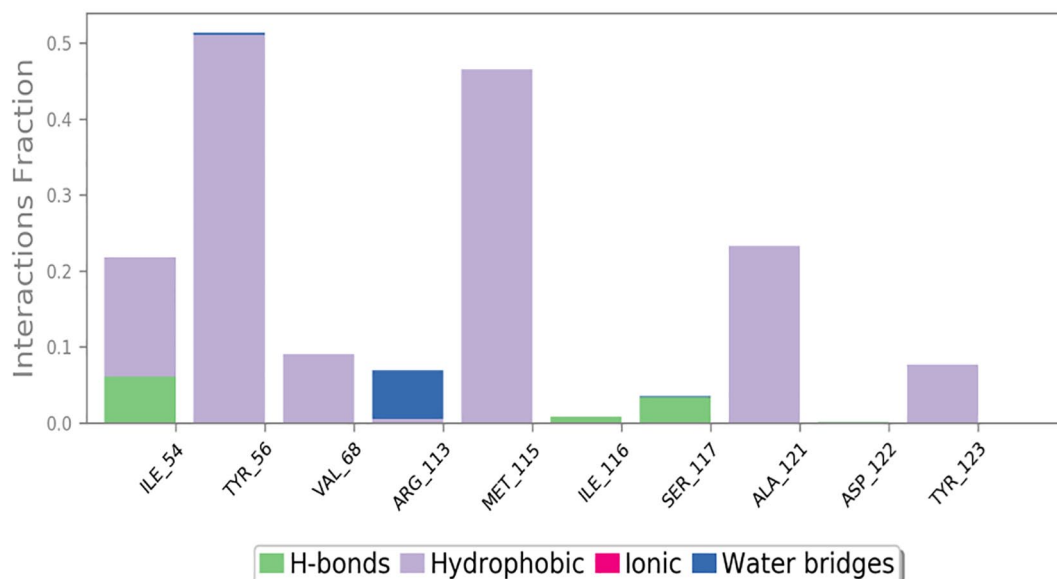


Figure 7. The protein-ligand interactions: (a) hydrogen bonds—green, hydrophobic—white purple, ionic—pink, water bridges—blue).

Table 4. Binding energy calculation of benzosampangine with PD-L1 and non-bonded interaction energies from MM-GBSA trajectories.

ENERGIES (KCAL/MOL)	BENZOSAMPANGINE-PD-L1
ΔG_{bind}	-39.39931414
$\Delta G_{\text{bindCoulomb}}$	-19.86215968
$\Delta G_{\text{bindCovalent}}$	1.762700362
$\Delta G_{\text{bindHbond}}$	-0.001425516
$\Delta G_{\text{bindLipo}}$	-23.83190531
$\Delta G_{\text{bindSolvGB}}$	33.50724005
$\Delta G_{\text{bindvdW}}$	-27.70691006

(ADMET) properties, positioning it as a promising candidate for in the development of effective cancer immunotherapy agents. Considering the advancement of PD-L1 inhibitors,⁶⁹ pyrvinium, an FDA-approved anthelmintic drug,⁷⁰ has demonstrated in vitro efficacy against the PD-L1 receptor,⁷¹ indicating potential for repurposing in cancer therapy. BMS-202, currently progressing through pre-clinical trials,⁷² shows early-stage promise, whereas CA-170's involvement in clinical research targeting NSCLC highlights its clinical relevance in oncology.^{73,74} These compounds, namely pyrvinium, BMS-202, and CA-170, serve as experimentally validated controls in our study. Nevertheless, the comprehensive evaluation of benzosampangine's ADMET characteristics suggests several potential advantages over the experimentally validated control molecules, including pyrvinium, BMS-202, and CA-170. These findings warrant further investigation into its suitability for development as a therapeutic targeting the PD-L1 pathway (Table 5). One promising feature of Benzosampangine is its

predicted favorable absorption profile, characterized by high intestinal absorption (HIA),⁷⁵ which surpasses that of pyrvinium and CA-170. This attribute is indicative of its potential for efficient systemic delivery and distribution within the body and is critical for achieving therapeutic efficacy. In addition, Benzosampangine is predicted to demonstrate an extensive volume of distribution, exceeding that of BMS-202, signifying its propensity to reach target tissues and maintain therapeutic concentrations, essential for triggering a robust antitumor response.⁷⁶ Its balanced logS value of -4.21 and logP value of 3.05 also surpass those of pyrvinium and BMS-202, further enhancing its pharmacokinetic profile and potential for optimal absorption and distribution across biological membranes.⁷⁷ Moreover, benzosampangine is predicted to demonstrate moderate blood-brain barrier (BBB) penetration, similar to that of pyrvinium and CA-170, and higher than of BMS-202 value, which may help mitigate the risk of central nervous system exposure and associated neurotoxicity.⁷⁸ In terms of predictive metabolic interactions, benzosampangine exhibits moderate activity as both a substrate and inhibitor of cytochrome P450 (CYP) enzymes, particularly CYP2D6 and CYP3A4, comparable to or better than the other molecules, potentially conferring advantages in terms of reduced susceptibility to metabolic degradation and drug-drug interaction modulation.⁷⁹ Furthermore, benzosampangine shows a low risk of hERG blocker toxicity distinguishes it from pyrvinium and BMS-202, indicating a lower potential for cardiac arrhythmia, a critical safety consideration in drug development.⁸⁰ The absence of PAINS alerts (pan-assay interference compounds) in benzosampangine's structural features is a significant computational advantage over pyrvinium, which exhibits 2 PAINS alerts. This absence may suggest a lower likelihood of off-target effects or undesirable interactions, enhancing the safety profile of

Table 5. ADMET properties of PD-L1 inhibitors.

ADMET PROPERTIES	BENZOSAMPANGINE	CA-170	PYRVINIUM	BMS-202	IDEAL RANGE/NOTES
Molecular Weight (MW)	282.08	360.32	382.23	419.22	<500 Da is favorable
TPSA	42.85	226.92	46.53	72.48	<140Å ² is favorable
logS	-6.886	-1.101	-5.12	-3.387	Higher values indicate better solubility
logP	4.309	-2.85	5.03	3.727	-0.4 to 5.6 is favorable
QED	0.403	0.238	0.436	0.488	Closer to 1 indicates higher drug-likeness
HIA	0.007	0.016	0.686	0.004	Low values indicate higher HIA
VD	1.014	0.396	0.432	1.873	Dependent on drug's target and therapeutic window
Lipinski Rule	Accepted	Rejected	Accepted	Accepted	No more than 1 violation
BBB Penetration	Moderate	Low	High	Moderate	High penetration desired for CNS drugs
CYP 2D6 Inhibitor	Low	Very Low	Moderate	High	Non-inhibitor preferred
CYP 3A4 Inhibitor	Moderate	Very Low	Moderate	High	Non-inhibitor preferred
hERG Blockers	Low	Very Low	Low	Moderate	Non-blocker preferred to avoid cardiac toxicity
Carcinogenicity	Low Risk	Low Risk	Low Risk	Low Risk	Non-carcinogenic preferred

Benzosampangine.⁸¹ Moreover, benzosampangine's docking score of -9.4 kcal/mol, indicate a strong molecular affinity for the PD-L1 receptor, surpassing those of the control compounds. The high recorded affinity supports the promising for potent and specific inhibitory action against the PD-L1 pathway, a pivotal mechanism implicated in tumor immune evasion.

Although BMS-202 and CA-170 are both currently in developmental phases, benzosampangine is standing out as a promising candidate for further investigations as a PD-L1 inhibitor given to its higher ADMET profile and exceptional docking score. Lower docking scores of -8.6 kcal/mol for BMS-202 and -6.5 kcal/mol for CA-170 suggest weaker molecular affinity for the PD-L1 receptor, supporting the hypothesis that benzosampangine could exhibit stronger molecular interactions and therapeutic potential (Table 6).

When comparing interactions of benzosampangine to control molecules (CA-170, BMS-202, and pyrvinium), it appears that benzosampangine may have the potential to mimic the roles of these control compounds and potentially surpass them in terms of binding stability and specificity. Figure 8 shows that all 4 molecules bind within the same pocket of the PD-L1 protein, suggesting that benzosampangine could exhibit similar inhibitory effects on the PD-L1/PD-1 interaction. CA-170 primarily relies on hydrogen bonds with SER117, ASN63, and GLN66, in addition to Van der Waals interactions and alkyl/Pi-alkyl interactions with residues such as VAL68 and ILE54

Table 6. Docking score against PD-L1.

MOLECULE	DOCKING SCORE (KCAL/MOL)
Benzosampangine	-9.4
Pyrvinium	-8.9
BMS-202	-8.6
CA-170	-6.5

(Figure 8B), whereas BMS-202 demonstrates a more diverse interaction profile, including hydrogen bonds and Pi-anion interaction with GLU58, Pi-Pi stacked and alkyl interactions with TYR56, Pi-sigma interaction with ILE54, as well as extensive Van der Waals interactions (Figure 8C). Despite the absence of hydrogen bonds, pyrvinium engages Pi-alkyl and alkyl interactions with residues such as TYR56, MET115, and ILE54, along with Van der Waals interactions and a carbon-hydrogen bond with ASP122 (Figure 8D). The unique combination of interactions observed in benzosampangine (Figure 8A), particularly the presence of triple Pi-sulfur interactions with MET115 and triple Pi-Pi stacked interactions with TYR56, suggests a potentially higher interaction profile. It is important to interpret the results of our investigation within this predictive framework, given that it was conducted using computational predictions. The robust interaction profile of benzosampangine indicates that it may exhibit strong

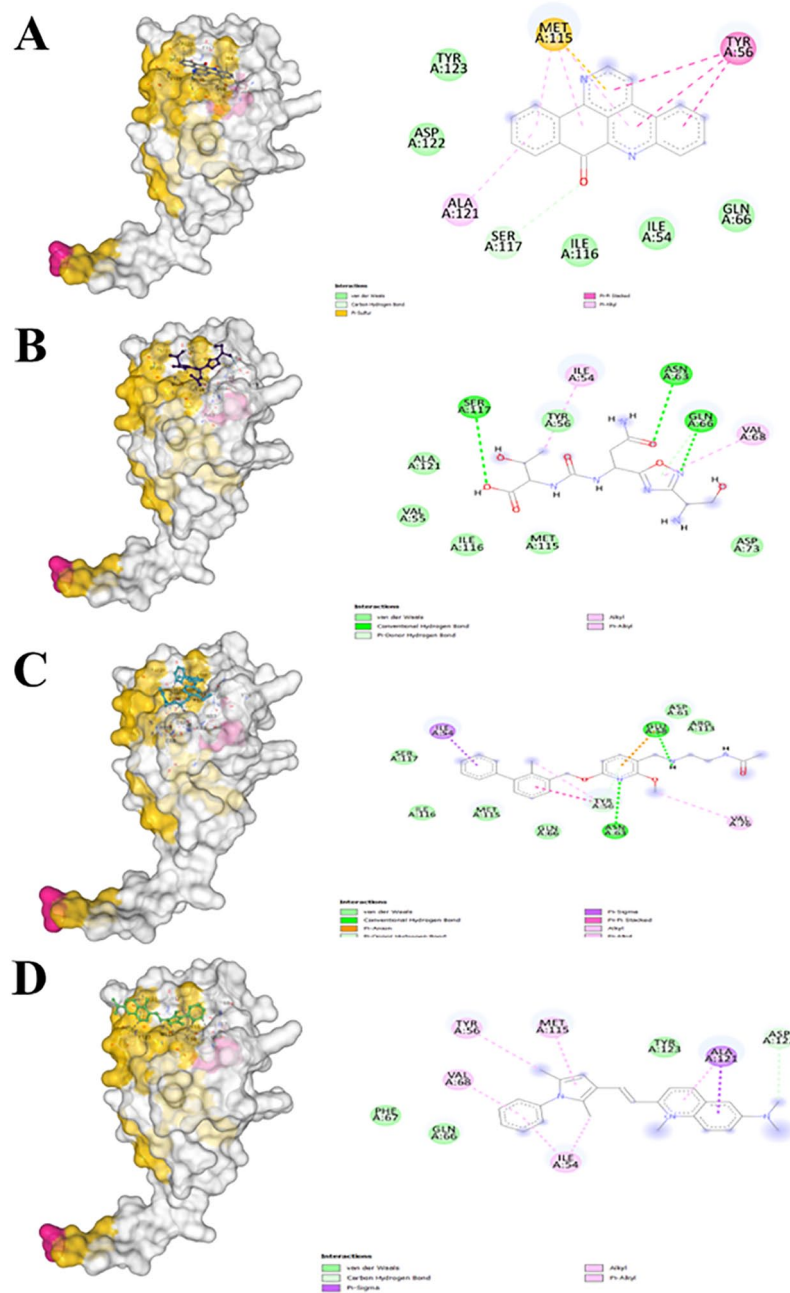


Figure 8. Binding pose and atomic-level interactions of control molecules CA-170 (B), BMS-202 (C), and pyrvinium (D) and benzosampanine (A).

inhibitory effects on the PD-L1/PD-1 pathway, potentially comparable to or probably exceeding those of CA-170, BMS-202, and pyrvinium.

When evaluating the system stability under physiological conditions, we compared the behavior of the benzosampanine-PD-L1 complex with that of the control molecule CA-170 in complex with PD-L1 over 100 ns of MD simulations. The CA-170-PD-L1 complex exhibits variations throughout the simulation time of 100 ns (Figure 9). Following an initial fluctuation due to equilibrium search, the RMSD of the complex

remains relatively stable around 12Å until 28 ns indicating that CA-170 initially maintains stability within the binding pocket of the protein. Then, several significant peaks in the RMSD of the CA-170-PD-L1 complex were observed up to approximately 72 ns, indicating that the ligand traveled a considerable distance from its initial position, thus revealing a period of instability of the ligand, probably due to its partial or complete detachment from its binding site on the protein. However, from around 73 ns onward, the RMSD decreases and remains stable without fluctuations toward the end of the simulation,

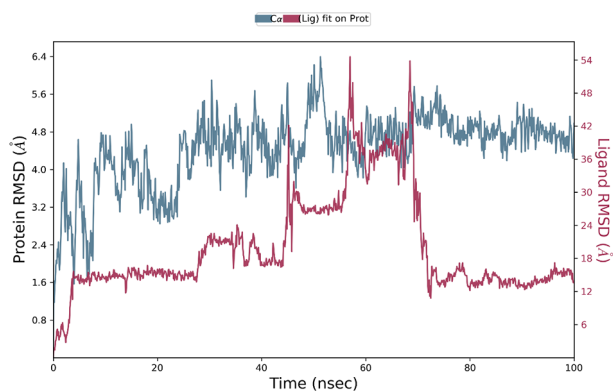


Figure 9. Root mean square deviation (RMSD) of the protein PD-L1 alone (blue) and in complex with CA-170 (red) as a function of simulation time.

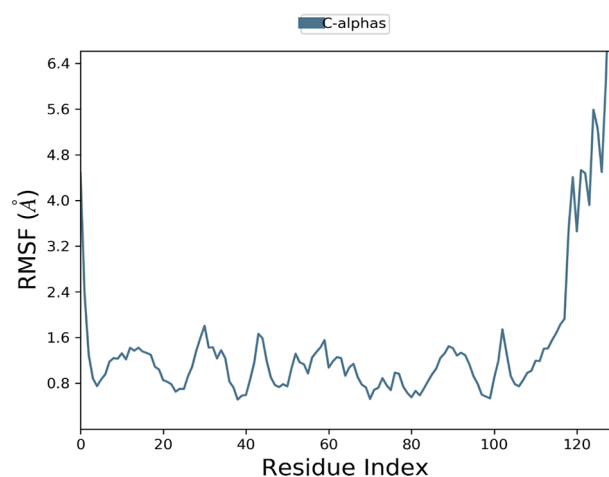


Figure 10. Root mean square fluctuation (RMSF) analysis of PD-L1 in complex with CA-170.

indicating that CA-170 regains its initial conformation and forms stable interactions with the protein. In contrast, benzosampangine does not exhibit such pronounced fluctuations and remains more stable in the protein binding pocket throughout the simulation. These results support the candidacy of benzosampangine as a promising ligand for therapeutic development targeting PD-L1. The RMSF plot of the CA-170-PD-L1 complex shows low RMSF values in the contact areas, indicating remarkable protein stability while bound to CA-170 (Figure 10). Similarly, the RMSF values for benzosampangine-PD-L1 complex are also low in these contact areas, showing that benzosampangine provides protein stability comparable to that of CA-170.

Discussion

We compared our observations with previous studies on PD-L1 inhibitors using computational approaches. Many previous studies have employed molecular docking to study the

interaction of PD-L1 with different inhibitors, and their reported results are consistent with ours regarding key residues involved in interactions that may induce inhibition.^{63,82,83} Our findings showed that benzosampangine interacts with the same binding site residues of PD-L1, namely MET115, TYR56, ALA121, SER117, TYR123, ASP122, ILE116, ILE54, and GLN66, confirming the relevance of our predictions. In addition, our study revealed hydrophobic interactions and stable hydrogen bonds between benzosampangine and these critical residues, which align with observations from previous studies.^{63,82,84} This alignment with previous works strengthens the credibility of our docking methodology and the validity of the identified interactions between benzosampangine and PD-L1. Furthermore, in the study by Sobral et al⁸⁵ identifying new PD-L1 inhibitors, it has been shown that effective inhibitors had binding energies of -9.213 and -8.023 kcal/mol, and specific interactions were recorded with PD-L1 domain. Our simulations yielded a similar trend, with benzosampangine exhibiting a binding free energy of -9.4 kcal/mol, suggesting its potential as a PD-L1 inhibitor. Furthermore, we compared our molecular dynamic simulation results with those of Kamal et al,⁸⁴ who analyzed the stability of PD-L1-inhibitors complexes using MD simulations. In their work, more RMSD fluctuations occurred, supporting the fact that the benzosampangine-PD-L1 complex maintains structural stability. Our MD simulations, conducted over a period of 100 ns, showed stable RMSD values around 1.52Å , indicating a stable conformation of the complex throughout the simulation. These results align with the Kamal research team's observations, where stable PD-L1 complexes with various inhibitors exhibited RMSD values below 2Å . In addition, the RMSD stability in our study is in agreement with Kumar et al,⁶⁶ who also found that stable PD-L1-inhibitor complexes showed RMSD fluctuations within a similar range (below 2.5Å). This outcome agreement reinforces the validity of our results, suggesting that benzosampangine forms a stable complex with PD-L1. We also analyzed the RMSF to identify residues with significant mobility in the complex. Residues such as Tyr56, Met115, and Ala121 in the PD-L1 pocket exhibited low RMSF values, indicating structural stability in the binding region, in line with Liang et al⁸⁶ who reported similar RMSF values for effective PD-L1 inhibitors. The low fluctuation of these critical residues supports the hypothesis that benzosampangine maintains a stable interaction with PD-L1. However, it is important to note that our study is purely computational, and based only on *in silico* data. While these results are promising, they remain hypothetical until validated through experimental studies. Overall, our findings confirm that benzosampangine forms a stable complex with PD-L1 by interacting with critical residues in the binding pocket, which are consistent with reference studies. Benzosampangine is a lead compound among 511 natural compounds identified through molecular docking and MD simulations, showing strong potential as a PD-L1

inhibitor. Nevertheless, further steps are required, such as in vitro validation of its inhibitory effects, followed by possible structural optimization to enhance its binding potential. In addition, preclinical and clinical studies will be essential to confirm its efficacy and safety.

Conclusions

Through the anticipated findings of benzosampangine, this study targets the PD-L1 pathway, offering a promising in cancer immunotherapy. According to comprehensive computational methods, benzosampangine has emerged as a compound exhibiting great potential, demonstrating a significant predicted binding affinity toward PD-L1, supported by favorable pharmacokinetic and ADMET properties. Its adherence to Ro5 suggests its potential as a drug candidate supported by its suitability for oral administration. Compared with control molecules such as CA-170 and BMS-202, benzosampangine showed favorable predicted molecular interactions and a superior ADMET profile, reinforcing its potential as a leading PD-L1 inhibitor. However, the transition from computational predictions to clinical application requires thorough experimental validation, including in vitro and in vivo studies, to confirm benzosampangine efficacy and mechanism of action in tumor immunity. Enhancing the pharmacological profile by improving its solubility, stability, and bioavailability, alongside developing effective delivery systems, will be essential for future therapeutic development. This approach could potentially elevate benzosampangine from a promising to a viable therapeutic candidate, emphasizing the critical role of computational methods in drug discovery. The study illustrates the potential of computational tools in identifying novel inhibitors, supporting the development of more efficient and cost-effective therapeutic solutions.

Acknowledgements

This study is part of a doctoral thesis with a scholarship from the Mohammed VI Foundation for Science and Health.

Author Contributions

Abderrahim Ait Ouchaoui and Salah Eddine El Hadad conceived the study, developed the methodology, performed in silico simulations, analyzed and organized data, and drafted the manuscript. Marouane Aherkou provided technical assistance and critically reviewed the methodology. Elkamili Fadoua assisted in the drafting of the manuscript, contributing to the organization and clarity of the content. Mkamel Mouad, Youssef Ramli and Anass Kettani conducted a thorough review of the manuscript, providing feedback and recommendations to enhance its content and clarity. Ilhame Bourais led the study design, and supervised the research process, conducted the final critical review and editing of the manuscript, finalized and approved the manuscript for submission.

ORCID iD

Ilhame Bourais  <https://orcid.org/0000-0002-4995-7837>

REFERENCES

- Catros-Quemener V, Bouet et Noëlle Genetet F. Immunité thérapies cellulaires du cancer. *Med Sci (Paris)*. 2003;19:43-53.
- Walker PR, Prins RM, Dietrich P-Y, Liau LM. Harnessing T-cell immunity to target brain tumors. In: Van Meir, EG, ed. *CNS Cancer*. Humana Press; 2009:1165-1217. doi:10.1007/978-1-60327-553-8_48
- Chen DS, Mellman I. Oncology meets immunology: the cancer-immunity cycle. *Immunity*. 2013;39:1-10. doi:10.1016/j.immuni.2013.07.012
- Lei Q, Wang D, Sun K, Wang L, Zhang Y. Resistance mechanisms of anti-PD1/PDL1 therapy in solid tumors. *Front Cell Dev Biol*. 2020;8:672. doi:10.3389/fcell.2020.00672
- Maimela NR, Liu S, Zhang Y. Fates of CD8+ T cells in tumor microenvironment. *Comput Struct Biotechnol J*. 2019;17:1-13. doi:10.1016/j.csbj.2018.11.004
- Garcia-Diaz A, Shin DS, Moreno BH, et al. Interferon receptor signaling pathways regulating PD-L1 and PD-L2 expression. *Cell Rep*. 2017;19:1189-1201. doi:10.1016/j.celrep.2017.04.031
- Ribas A. Adaptive immune resistance: how cancer protects from immune attack. *Cancer Discov*. 2015;5:915-919. doi:10.1158/2159-8290.CD-15-0563
- Agata Y, Kawasaki A, Nishimura H, et al. Expression of the PD-1 antigen on the surface of stimulated mouse T and B lymphocytes. *Int Immunol*. 1996;8:765-772. doi:10.1093/intimm/8.5.765
- Ribas A, Wolchok JD. Cancer immunotherapy using checkpoint blockade. *Science*. 2018;359:1350-1355. doi:10.1126/science.aar4060
- Akinleye A, Rasool Z. Immune checkpoint inhibitors of PD-L1 as cancer therapeutics. *J Hematol Oncol*. 2019;12:1-13. doi:10.1186/s13045-019-0779-5
- Brahmer JR, Tykodi SS, Chow LQM, et al. Safety and activity of anti-PD-L1 antibody in patients with advanced cancer. *N Engl J Med*. 2012;366:2455-2465. doi:10.1056/nejmoa1200694
- Patel SP, Kurzrock R. PD-L1 expression as a predictive biomarker in cancer immunotherapy. *Mol Cancer Ther*. 2015;14:847-856. doi:10.1158/1535-7163.MCT-14-0983
- Chen G, Huang AC, Zhang W, et al. Exosomal PD-L1 contributes to immunosuppression and is associated with anti-PD-1 response. *Nature*. 2018;560:382-386. doi:10.1038/s41586-018-0392-8
- Bellucci R, Martin A, Bommarito D, et al. Interferon- γ -induced activation of JAK1 and JAK2 suppresses tumor cell susceptibility to NK cells through upregulation of PD-L1 expression. *Oncotarget*. 2015;4:e1008824. doi:10.1080/2162402X.2015.1008824
- Kim JM, Chen DS. Immune escape to PD-L1/PD-1 blockade: seven steps to success (or failure). *Ann Oncol*. 2016;27:1492-1504. doi:10.1093/annonc/mdw217
- Jiang X, Wang J, Deng X, et al. Role of the tumor microenvironment in PD-L1/PD-1-mediated tumor immune escape. *Mol Cancer*. 2019;18:10.
- Keir ME, Butte MJ, Freeman GJ, Sharpe AH. PD-1 and its ligands in tolerance and immunity. *Annu Rev Immunol*. 2008;26:677-704. doi:10.1146/annurev.immunol.26.021607.090331
- Nguyen LT, Ohashi PS. Clinical blockade of PD1 and LAG3—potential mechanisms of action. *Nat Rev Immunol*. 2015;15:45-56. doi:10.1038/nri3790
- Zou W, Wolchok JD, Chen L. PD-L1 (B7-H1) and PD-1 pathway blockade for cancer therapy: mechanisms, response biomarkers, and combinations. *Sci Transl Med*. 2016;8:328rv4.
- Hematol J, Yi M, Niu M, Xu L, Luo S, Wu K. Regulation of PD-L1 expression in the tumor microenvironment. *J Hematol Oncol*. 2021;14:10. doi:10.1186/s13045-020-01027-5
- Topalian SL, Drake CG, Pardoll DM. Targeting the PD-1/B7-H1 (PD-L1) pathway to activate anti-tumor immunity. *Curr Opin Immunol*. 2011;24:207-212. doi:10.1016/j.coi.2011.12.009
- Kemeny HR, Elsamadicy AA, Farber SH, et al. Targeting PD-L1 initiates effective antitumor immunity in a murine model of Cushing disease. *Clin Cancer Res*. 2020;26:1141-1151. doi:10.1158/1078-0432.CCR-18-3486
- Powles T, Eder JP, Fine GD, et al. Activity in metastatic bladder cancer. *Nature*. 2014;515:558-562. doi:10.1038/nature13904
- Gandini S, Massi D, Mandalà M. PD-L1 expression in cancer patients receiving anti PD-1/PD-L1 antibodies: a systematic review and meta-analysis. *Crit Rev Oncol Hematol*. 2016;100:88-98. doi:10.1016/j.critrevonc.2016.02.001
- Monneur A, Gonçalves A, Bertucci F. Expression de PD-L1 et inhibiteurs de la voie PD-1/PD-L1 dans le cancer du sein. *Bull Cancer*. 2018;105:263-274. doi:10.1016/j.bulcan.2017.11.012
- Coyne GOS, Madan RA, Gulley JL. Nivolumab: promising survival signal coupled with limited toxicity raises expectations. *J Clin Oncol*. 2023;32:986-988.

27. Park JE, Kim E, Keam B, et al. Anti-tumor effects of NK cells and anti-PDL1 antibody with antibody-dependent cellular cytotoxicity in PD-L1-positive cancer cell lines. *J Immunother Cancer*. 2020;8:e000873. doi:10.1136/jitc-2020-000873
28. Vasant A, Jeffrey B. PD-1 and PD-L1 antibodies in cancer: current status and future directions. *Cancer Immunol Immunother*. 2017;66:551-564. doi:10.1007/s00262-017-1954-6
29. Dutriaux C, Maio M, Mortier L, et al. Nivolumab in previously untreated melanoma without BRAF mutation. *N Engl J Med*. 2015;372:320-330. doi:10.1056/NEJMoa1412082
30. Crinò L, Eberhardt WEE, Poddubskaya E, et al. Nivolumab versus docetaxel in advanced squamous-cell non-small-cell lung cancer. *N Engl J Med*. 2015;373:123-135. doi:10.1056/NEJMoa1504627
31. Herbst RS, Baas P, Kim D-W, et al. Pembrolizumab versus docetaxel for previously treated, PD-L1-positive, advanced non-small-cell lung cancer (KEYNOTE-010): a randomised controlled trial. *Lancet*. 2016;387:1540-1550. doi:10.1016/S0140-6736(15)01281-7
32. Leigh N, Balmanoukian AS, Eder JP, et al. Pembrolizumab for the treatment of non-small-cell lung cancer. *N Engl J Med*. 2018;372:2018-2028. doi:10.1056/NEJMoa1501824
33. Inman BA, Longo TA, Ramalingam S, Harrison MR. Atezolizumab: a PD-L1-blocking antibody for bladder cancer. *Clin Cancer Res*. 2017;23:1886-1890. doi:10.1158/1078-0432.CCR-16-1417
34. Dirix LY, Takacs J, Jerusalem G, et al. Avelumab, an anti-PD-L1 antibody, in patients with locally advanced or metastatic breast cancer: a phase 1b JAVELIN solid tumor study. *Breast Cancer Res Treat*. 2018;167:671-686. doi:10.1007/s10549-017-4537-5
35. Collins JM, Gulley JL, Collins JM, Gulley JL. Product review: avelumab, an anti-PD-L1 antibody product review: avelumab, an anti-PD-L1 antibody. *Hum Vaccin Immunother*. 2019;15:891-908. doi:10.1080/21645515.2018.1551671
36. Zanella A, Bortolotti M, Maiello S, Bolognesi A, Polito L. Anti-PD-L1 immunonjugates for cancer therapy: are available antibodies good carriers for toxic payload delivering? *Front Pharmacol*. 2022;13:972046. doi:10.3389/fphar.2022.972046
37. Chames P, Regenmortel M, Van Weiss E, Baty D. Therapeutic antibodies: successes, limitations and hopes for the future. *Br J Pharmacol*. 2009;157:220-233. doi:10.1111/j.1476-5381.2009.00190.x
38. Hansel TT, Kropshofer H, Singer T, Mitchell JA, George AJT. The safety and side effects of monoclonal antibodies. *Nat Publ Gr*. 2010;9:325-338. doi:10.1038/nrd3003
39. Delaney N, Michot J-M, Comont T, et al. Haematological immune-related adverse events induced by anti-PD-1 or anti-PD-L1 immunotherapy: a descriptive observational study. *Lancet Haematol*. 2019;6:e48-e57. doi:10.1016/S2352-3026(18)30175-3
40. Dos Santos-Silva CA, Zupin L, Oliveira-Lima M, et al. Plant antimicrobial peptides: state of the art, in silico prediction and perspectives in the omics era. *Bioinform Biol Insights*. 2020;14:1177932220952739. doi:10.1177/1177932220952739
41. Ali A, Ali M, Nisar Z, et al. Antibacterial activity of economically important medicinal plants in Pakistan against different bacterial strains. *Bioinform Biol Insights*. 2023;17:11779322231189374. doi:10.1177/11779322231189374
42. Nouadi B, Ezaouine A, El Messal M, Blaghen M, Bennis F, Chegani F. Prediction of anti-COVID 19 therapeutic power of medicinal Moroccan plants using molecular docking. *Bioinform Biol Insights*. 2021;15:11779322211009199. doi:10.1177/11779322211009199
43. Mathew S, Faheem M, Archunan G, et al. In silico studies of medicinal compounds against hepatitis C capsid protein from north India. *Bioinform Biol Insights*. 2014;8:159-168. doi:10.4137/BBI.S15211
44. Kolb P, Ferreira RS, Irwin JJ, Shoichet BK. Docking and chemoinformatic screens for new ligands and targets. *Curr Opin Biotechnol*. 2009;20:429-436. doi:10.1016/j.copbio.2009.08.003
45. El Mchichi L, Tabti K, Kasmir R, et al. 3D-QSAR study, docking molecular and simulation dynamic on series of benzimidazole derivatives as anti-cancer agents. *J Indian Chem Soc*. 2022;99:100582. doi:10.1016/j.jics.2022.100582
46. Zaki H, Belhassan A, Benlyas M, Lakhliif T, Bouachrine M. New dehydroabiestic acid (DHA) derivatives with anticancer activity against HepG2 cancer cell lines as a potential drug targeting EGFR kinase domain. *J Biomol Struct Dyn*. 2021;39:2993-3003. doi:10.1080/07391102.2020.1759452
47. Aissaoui S, Hajjia H, Zaki H, et al. Study of the anticancer potential of cannabidiol using computational methods. *Phys Chem Res*. 2024;12:783-800. doi:10.22036/pcr.2024.425179.2450
48. Abdel-Maksoud MA, Askar MA, Abdel-Rahman IY, Gharib M, Aufy M. Integrating network pharmacology and molecular docking approach to elucidate the mechanism of *Commiphora wightii* for the treatment of rheumatoid arthritis. *Bioinform Biol Insights*. 2024;18:11779322241247634. doi:10.1177/11779322241247634
49. Chujan S, Vajeethaveesin N, Satayavivad J, Kitkumthorn N. Identification of molecular mechanisms of ameloblastoma and drug repositioning by integration of bioinformatics analysis and molecular docking simulation. *Bioinform Biol Insights*. 2024;18:11779322241256459. doi:10.1177/11779322241256459
50. Wang Y, Bryant SH, Cheng T, et al. PubChem BioAssay: 2017 update. *Nucleic Acids Res*. 2017;45:D955-D963. doi:10.1093/nar/gkw1118
51. Morris GM, Huey R, Olson AJ. UNIT using AutoDock for ligand-receptor docking. *Curr Protoc Bioinformatics*. 2008;24:8-14. doi:10.1002/0471250953.bi0814s24
52. Liu Y, Yang X, Gan J, Chen S, Xiao Z-X, Cao Y. CB-Dock2: improved protein-ligand blind docking by integrating cavity detection, docking and homologous. *Nucleic Acids Res*. 2022;50:W159-W164.
53. Daina A, Michielin O, Zoete V. SwissADME: a free web tool to evaluate pharmacokinetics, drug-likeness and medicinal chemistry friendliness of small molecules. *Sci Rep*. 2017;7:42717. doi:10.1038/srep42717
54. Lipinski CA, Lombardo F, Dominy BW, Feeney PJ. Experimental and computational approaches to estimate solubility and permeability in drug discovery and development settings. *Adv Drug Deliv Rev*. 1997;23:3-25.
55. Iheagwam FN, Ogunlana OO, Ogunlana OE, Isewon I, Oyelade J. Potential anti-cancer flavonoids isolated from *Caesalpinia bonduc* young twigs and leaves: molecular docking and in silico studies. *Bioinform Biol Insights*. 2019;13:1177932218821371. doi:10.1177/1177932218821371
56. Banerjee P, Eckert AO, Schrey AK, Preissner R. ProTox-II: a webserver for the prediction of toxicity of chemicals. *Nucleic Acids Res*. 2018;46:257-263. doi:10.1093/nar/gky318
57. Modeling LS. (2008). *Life Science Modeling and Simulations*. Discovery Studio.
58. Rasheed MA, Iqbal MN, Saddick S, et al. Identification of lead compounds against scm (Fms10) in enterococcus faecium using computer aided drug designing. *Life*. 2021;11:1-15. doi:10.3390/life11020077
59. Ferreira LG, Dos Santos RN, Oliva G, Andricopulo AD. Molecular docking and structure-based drug design strategies. *Molecules*. 2015;20:13384-13421. doi:10.3390/molecules200713384
60. Shivakumar D, Williams J, Wu Y, Damm W, Shelley J, Sherman W. Prediction of absolute solvation free energies using molecular dynamics free energy perturbation and the opl force field. *J Chem Theory Comput*. 2010;6:1509-1519. doi:10.1021/ct900587b
61. Ylilauri M, Pentikäinen OT. MMGBSA as a tool to understand the binding affinities of filament-peptide interactions. *J Chem Inf Model*. 2013;53:2626-2633. doi:10.1021/ci4002475
62. Xiong G, Wu Z, Yi J, et al. ADMETlab 2.0: an integrated online platform for accurate and comprehensive predictions of ADMET properties. *Nucleic Acids Res*. 2021;49:W5-W14. doi:10.1093/nar/gkab255
63. Almahmoud S, Zhong HA. Molecular modeling studies on the binding mode of the PD-1/PD-L1 complex inhibitors. *Int J Mol Sci*. 2019;20:4654.
64. Wu X, Wang N, Liang J, Wang B. Is the triggering of PD-L1 dimerization a potential mechanism for food-derived small molecules in cancer immunotherapy? A study by molecular dynamics. *Int J Mol Sci*. 2023;24:1413.
65. Zak KM, Grudnik P, Guzik K, et al. Structural basis for small molecule targeting of the programmed death ligand 1 (PD-L1). *Oncotarget*. 2016;7:30323-30335.
66. Kumar GS, Moustafa M, Sahoo AK, Mal P. Computational investigations on the natural small molecule as an inhibitor of programmed death ligand 1 for cancer immunotherapy. *Life (Basel)*. 2022;12:659.
67. Skalniak L, Zak KM, Guzik K, et al. Small-molecule inhibitors of PD-1/PD-L1 immune checkpoint alleviate the PD-L1-induced exhaustion of T-cells. *Oncotarget*. 2017;8:72167-72181.
68. Elkamili F, Ait Ouchauoui A, Lorente-Leyva LL, Peluffo-Ordóñez DH. High-throughput virtual screening approach and dynamic simulation of natural compounds as target inhibitors of BACE1 in Alzheimer's disease. *F1000Res*. 2023;12:1392. doi:10.12688/f1000research.140568.1
69. Wu Q, Jiang L, Li S-C, He Q-J, Yang B, Cao J. Small molecule inhibitors targeting the PD-1/PD-L1 signaling pathway. *Acta Pharmacol Sin*. 2021;42:1-9. doi:10.1038/s41401-020-0366-x
70. Schultz CW, Nevler A. Pyrvinium pamoate: past, present, and future as an anti-cancer drug. *Biomedicines*. 2022;10:1-16. doi:10.3390/biomedicines10123249
71. Fattakhova E, Hofer J, DiFlumeri J, et al. Identification of the FDA-approved drug pyrvinium as a small-molecule inhibitor of the PD-1/PD-L1 interaction. *ChemMedChem*. 2021;16:2769-2774. doi:10.1002/cmdc.202100264
72. Song Z, Liu B, Peng X, et al. Design, synthesis, and pharmacological evaluation of biaryl-containing PD-1/PD-L1 interaction inhibitors bearing a unique difluoromethyleneoxy linkage. *J Med Chem*. 2021;64:16687-16702. doi:10.1021/acs.jmedchem.1c01422
73. Li T-T, Jiang J-W, Qie C-X, et al. Identification of active small-molecule modulators targeting the novel immune checkpoint VISTA. *BMC Immunol*. 2021;22:55. doi:10.1186/s12865-021-00446-4
74. Hagemann IS, Devarakonda S, Lockwood CM, et al. Clinical next-generation sequencing in patients with non-small cell lung cancer. *Cancer*. 2015;121:631-639. doi:10.1002/cncr.29089
75. Basant N, Gupta S, Singh KP. Predicting human intestinal absorption of diverse chemicals using ensemble learning based QSAR modeling approaches. *Comput Biol Chem*. 2016;61:178-196. doi:10.1016/j.compbiolchem.2016.01.005

76. Holt K, Nagar S, Korzekwa K. Methods to predict volume of distribution. *Curr Pharmacol Rep.* 2019;5:391-399. doi:10.1007/s40495-019-00186-5
77. Lipinski CA, Lombardo F, Dominy BW, Feeney PJ. Experimental and computational approaches to estimate solubility and permeability in drug discovery and development settings. *Adv Drug Deliv Rev.* 2012;64:4-17. doi:10.1016/j.addr.2012.09.019
78. Yuan Y, Zheng F, Zhan CG. Improved prediction of blood-brain barrier permeability through machine learning with combined use of molecular property-based descriptors and fingerprints. *AAPS J.* 2018;20:15-17. doi:10.1208/s12248-018-0215-8
79. Lynch T, Price A. The effect of cytochrome P450 metabolism on drug response, interactions, and adverse effects. *Am Fam Physician.* 2007;76:391-396.
80. Creanza TM, Delre P, Ancona N, Lentini G, Saviano M, Mangiatordi GF. Structure-based prediction of hERG-related cardiotoxicity: a benchmark study. *J Chem Inf Model.* 2021;61:4758-4770. doi:10.1021/acs.jcim.1c00744
81. Azzouzi M, Azougagh O, Ouchaoui AA, et al. Synthesis, characterizations, and quantum chemical investigations on imidazo[1,2-a]pyrimidine-Schiff base derivative: (E)-2-phenyl-N-(thiophen-2-ylmethylene)imidazo[1,2-a]pyrimidin-3-amine. *ACS Omega.* 2023;9:837-857. doi:10.1021/acsomega.3c06841
82. Fantacuzzi M, Paciotti R, Agamennone M. A comprehensive computational insight into the PD-L1 binding to PD-1 and small molecules. *Pharmaceuticals.* 2024;17:316. doi:10.3390/ph17030316
83. Wang F, Ye W, Wang S, et al. Discovery of a new inhibitor targeting PD-L1 for cancer immunotherapy. *Neoplasia.* 2021;23:281-293. doi:10.1016/j.neo.2021.01.001
84. Kamal MA, Badary HA, Omran D, et al. Virtual screening and biological evaluation of potential PD-1/PD-L1 immune checkpoint inhibitors as anti-hepatocellular carcinoma agents. *ACS Omega.* 2023;8:33242-33254. doi:10.1021/acsomega.3c00279
85. Sobral PS, Luz VCC, Almeida JMGCF, Videira PA, Pereira F. Computational approaches drive developments in immune-oncology therapies for PD-1/PD-L1 immune checkpoint inhibitors. *Int J Mol Sci.* 2023;24:5908. doi:10.3390/ijms24065908
86. Liang J, Wang B, Yang Y, Liu B, Jin Y. Approaching the dimerization mechanism of small molecule inhibitors targeting PD-L1 with molecular simulation. *Int J Mol Sci.* 2023;24:1280. doi:10.3390/ijms24021280